Free Waves on Barotropic Vortices. Part I: Eigenmode Structure

MICHAEL T. MONTGOMERY

Department of Atmospheric Science, Colorado State University, Fort Collins, Colorado

CHUNGU LU

Forecast Systems Laboratory, NOAA/ERL, Boulder, Colorado

(Manuscript received 1 April 1996, in final form 27 November 1996)

ABSTRACT

To understand the nature of coupling between a hurricane vortex and asymmetries in its near-core region, it is first necessary to have an understanding of the spectrum of free waves on barotropic vortices. As foundation for upcoming work examining the nonaxisymmetric initial-value problem in inviscid and swirling boundary layer vortex flows, the complete spectrum of free waves on barotropic vortices is examined here.

For a variety of circular vortices in gradient balance the linearized momentum and continuity equations are solved as a matrix eigenvalue problem for perturbation height and wind fields. Vortex eigensolutions are found to fall into two continuum classes. Eigenmodes with frequencies greater than the advective frequency for azimuthal wavenumber n are modified gravity–inertia waves possessing nonzero potential vorticity in the near-core region. Eigenmodes whose frequencies scale with the advective frequency comprise both gravity–inertia waves and Rossby–shear waves. Linearly superposing the Rossby–shear waves approximates the sheared disturbance solutions. For wavenumbers greater than a minimum number, Rossby–shear waves exhibit gravity wave characteristics in the near-vortex region. Although such eigenstructure changes are not anticipated by traditional scaling analyses using solely external flow parameters, a criterion extending Rossby's characterization of ''balanced'' and ''unbalanced'' flow to that of azimuthal waves on a circular vortex is developed that correctly predicts the observed behavior from incipient vortices to hurricane-like vortices. The criterion is consistent with asymmetric balance theory. Possible applications of these results to the wave-mean-flow dynamics of geophysical vortex flows are briefly discussed.

1. Introduction

Above the boundary layer the hurricane can be meaningfully idealized as a circular vortex in gradient balance plus small-amplitude asymmetries (Shapiro and Montgomery 1993, Fig. 1). The source for the asymmetries is a combination of synoptic-scale forcing, turbulent stress at the sea surface, and cumulus convection. Despite extensive hurricane modeling using three-dimensional primitive equation models, surprisingly little is known about the nature of coupling between asymmetries and the mean vortex in rapidly rotating (large Rossby number) divergent flow regimes. To fix ideas, suppose at time zero a circular vortex is subject to a small but finite-amplitude asymmetric disturbance in both mass and wind fields near its radius of maximum winds. In general, the initial disturbance will excite radiating gravity waves and shear waves on the vortex. Do the excited waves interact with the mean vortex in the near-core region? If significant interaction occurs, then can one meaningfully quantify its dependence on the wave amplitude, the Rossby number, and the Froude number? Since forcing mechanisms in hurricanes exist on a spectrum of length scales, it is also of meteorological interest to be able to quantify the dependence of the interaction on the radial and azimuthal scales of the initial disturbance. In the first approximation, the ensuing adjustment may be represented by a superposition over the free eigensolutions of a circular vortex in gradient balance. Because interaction among these modes ultimately determines the mean flow coupling at second order in wave amplitude, understanding the structure of free waves on barotropic vortices is a necessary prerequisite. Thus, as a foundation for future investigations of the wave-mean-flow dynamics in barotropic and baroclinic vortices, this work examines the structure of free waves on barotropic vortices representative of hurricanes.

Knowledge of the wave spectrum in a spherical envelope of rotating fluid on a resting basic state has provided valuable insight into the dynamics of the tropical atmosphere (Matsuno 1966; Lindzen 1967; Longuet-Higgins 1968; Gill 1982). In contrast, our understanding of the wave spectrum in rapidly rotating vortices, such

Corresponding author address: Dr. Michael T. Montgomery, Department of Atmospheric Science, Colorado State University, Fort Collins, CO 80523.
E-mail: mtm@charney.atmos.colostate.edu

as hurricanes and polar lows, is incomplete. Previous studies have emphasized the identification of exponential instabilities and forced waves in hurricane-like vortices (Kurihara 1976; Fung 1977; Willoughby 1977; Flatau and Stevens 1989; Ford 1994) and ocean-ring vortices (Dewar and Killworth 1995). But little attention has been given to elucidating the physics of neutral gravity-wave and neutral shear-wave disturbances in barotropic vortex flows, which are necessary for completing the solution to the nonaxisymmetric initial-value problem. In light of renewed interest in the application of balance models to complex geophysical flows (Spall and McWilliams 1992; Shapiro and Montgomery 1993), classification of the vortex eigenspectrum into ''balanced'' and ''unbalanced'' flow is also of some theoretical interest. Such a classification is straightforward on a resting basic state since a clear timescale separation between ''fast'' (gravity–inertia) and ''slow'' (geostrophic/Rossby) modes exists. In the rapidly rotating region of an intense vortex, however, a well-defined timescale separation generally does not exist.

The outline of the paper is as follows. To facilitate the interpretation of vortex eigenmodes, section 2 reviews the well-known properties of linearized eigenstates on a resting basic state. Section 3 summarizes the formulation of the matrix eigenvalue problem and the construction of the nonresting basic states. Section 4 presents vortex eigenspectra. Section 5 presents vortex eigenmode structures for several swirl profiles, and key results are interpreted using a monochromatic generalization of Rossby's adjustment problem. Section 6 briefly considers the nonaxisymmetric adjustment problem and it is demonstrated that superposing over all modes yields radially propagating gravity–inertia waves and vortex–Rossby waves. Section 7 summarizes the results and indicates avenues for future work.

2. Free waves on a resting basic state revisited

To facilitate the interpretation of vortex eigenmode structures on a rapidly rotating vortex, we consider a variation of Kelvin's problem (Thomson 1879) on the small-amplitude gravitational oscillations in rotating shallow water. Although the main results are well known, a brief review proves useful in upcoming sections. If the curvature of the free surface is neglected, the linearized f-plane shallow-water equations in cylindrical coordinates are

$$\frac{\partial u'}{\partial t} - fv' + g\frac{\partial h'}{\partial r} = 0, \tag{2.1a}$$

$$\frac{\partial v'}{\partial t} + fu' + g\frac{\partial h'}{r\partial\lambda} = 0, \tag{2.1b}$$

$$\frac{\partial h'}{\partial t} + H\left[\frac{\partial}{r\partial r}(ru') + \frac{\partial v'}{r\partial\lambda}\right] = 0. \tag{2.1c}$$

Here, f denotes a constant Coriolis parameter; g is gravitational acceleration; H is a constant resting depth; h' is surface-height perturbation; and (u', v') are perturbation radial and tangential winds, respectively. Other notation is standard. The flow domain occupies the circular region $0 \le r \le a$. Perturbation quantities are assumed finite at $r = 0$, while the height perturbation is assumed to vanish at $r = a$. Vanishing height is preferred over a vanishing radial velocity at $r = a$ since the limit $a \to \infty$ corresponding to the unbounded domain is obtained most simply.

Free waves of (2.1) are obtained via the modal ansatz

$$(u', v', h') = (\hat{u}(r), \hat{v}(r), \hat{h}(r))\exp[i(n\lambda - \sigma t)], \tag{2.2}$$

where n denotes the azimuthal wavenumber and σ the wave frequency. In azimuthal-Fourier space the linearized disturbance equations (2.1) can be written as a matrix equation

$$\begin{pmatrix} \sigma & f & -g\dfrac{d}{dr} \\ f & \sigma & -n\dfrac{g}{r} \\ \dfrac{H}{r}\dfrac{d}{dr}r & -\dfrac{nH}{r} & \sigma \end{pmatrix}\begin{pmatrix} i\hat{u} \\ \hat{v} \\ \hat{h} \end{pmatrix} = 0, \tag{2.3}$$

which possesses three manifolds of solutions. The first manifold corresponds to steady geostrophic flow ($\sigma = 0$) in which the Coriolis force is balanced by the pressure gradient force

$$f\hat{v} = g\frac{\partial\hat{h}}{\partial r}, \tag{2.4a}$$

$$f\hat{u} = \frac{-in}{r}g\hat{h}. \tag{2.4b}$$

Here, $g\hat{h}/f$ is a streamfunction for the geostrophic wind. Vorticity ($\hat{\zeta}$) and potential vorticity ($\hat{P}$) amplitudes are given by

$$\hat{\zeta} = \frac{d}{rdr}(r\hat{v}) - \frac{in}{r}\hat{u}$$

$$= \frac{g}{f}\hat{\nabla}^2\hat{h}, \tag{2.4c}$$

$$\hat{P} = \frac{\hat{\zeta}}{H} - f\frac{\hat{h}}{H^2}$$

$$= \frac{g}{fH}\{\hat{\nabla}^2\hat{h} - \gamma^2\hat{h}\}, \tag{2.4d}$$

where $\hat{\nabla}^2 = d/rdr(rd/dr) - n^2/r^2$ is the horizontal Laplacian in azimuthal-Fourier space and $\gamma^2 = f^2/gH$ is the inverse square of the Rossby radius of deformation. For isolated disturbances, $\hat{\zeta}$ and $\hat{P}$ are anticorrelated with $\hat{h}$.

Had the parabolic free surface associated with the rotating annulus not been neglected in (2.1), the geostrophic modes would become Rossby waves (Phillips 1965). For small free-surface slopes, these waves ret-

rogress in the rotating frame, possess small frequencies compared to the rotation frequency, and are well described by quasigeostrophic dynamics. The Rossby wave vorticity and potential vorticity (PV) are again anticorrelated with the height

$$\zeta' \propto -h',$$
$$P' \propto -h'. \tag{2.5}$$

Superposing the geostrophic and iso-allobaric winds shows that the total wind lags the height contours. The propagation of a monochromatic Rossby wave around the annulus can then be interpreted as an adjustment process whereby wind adjusts to mass,

$$\text{wind} \rightarrow \text{mass}, \tag{2.6}$$

where mass represents the perturbation height and wind represents the total perturbation wind.

On letting $\beta_{\text{eff}} = f/HdH/dr$, the local dispersion relation for topographic Rossby waves in an annulus takes the form

$$\sigma = \frac{-\frac{n}{r}\beta_{\text{eff}}}{k^2 + \frac{n^2}{r^2} + \frac{f^2}{gH}}, \tag{2.7}$$

where σ is wave frequency and k is radial wavenumber. For sufficiently small free-surface slopes, Rossby waves possess frequencies smaller than f, therefore

$$\sigma^2 < f^2. \tag{2.8}$$

Substituting (2.7) into (2.8) yields

$$L^2 > \frac{c^2}{f^2}, \tag{2.9}$$

where $L = r/n$, the characteristic azimuthal length scale for azimuthal wavenumber n, and $c = \sigma r/n$, the azimuthal Rossby wave phase speed. Because (2.9) is formally identical to Rossby's adjustment criterion for balanced flow, it suggests a useful interpretation of linearized Rossby wave dynamics. Rewriting (2.9) yields

$$\frac{L^2}{c^2} > \frac{1}{f^2}, \tag{2.10}$$

indicating that if the wave timescale is sufficiently long the Coriolis force can effectively rotate the wind vectors, and thus wind adjusts to mass. Such wave disturbances are regarded as balanced and are customarily identified with the slow manifold.

Returning to the constant depth model (2.3), the second and third solutions are unsteady ($\sigma \neq 0$). In this case, (2.3) may be solved by eliminating winds in favor of height yielding a simplified Tidal equation

$$\frac{d^2\hat{h}}{dr^2} + \frac{1}{r}\frac{d\hat{h}}{dr} + \left(\kappa^2 - \frac{n^2}{r^2}\right)\hat{h} = 0, \tag{2.11}$$

where κ represents the eigenvalue for azimuthal wavenumber n. The frequency σ is determined from the dispersion relation for gravity–inertia waves (Poincaré waves),

$$\sigma^2 = f^2 + \kappa^2 gH. \tag{2.12}$$

Solutions to (2.11) that are bounded at $r = 0$ are given by

$$\hat{h}(r) = AJ_n(\kappa r), \tag{2.13}$$

where J_n is the Bessel function of the first kind of order n and A is an arbitrary amplitude. The outer boundary condition $\hat{h}(a) = 0$ furnishes discrete eigenvalues (κ_j; $j = 1, 2, \ldots$) for each azimuthal wavenumber n. The dispersion relation (2.12) then yields a positive and negative frequency for each j. As a is increased, so as to better approximate an unbounded domain, the eigenfrequencies (2.12) become more closely spaced and ultimately approach a twofold continuum as $a \rightarrow \infty$. Nonaxisymmetric modes ($n = 1, 2, \ldots$) with $\sigma > 0$ propagate around the origin in a counterclockwise sense, (progress relative to f), while nonaxisymmetric modes with $\sigma < 0$ propagate around the origin in a clockwise sense (retrogress relative to f). Velocity amplitudes follow from the polarization relations

$$i\hat{u} = \frac{\left(\frac{-nf}{r}g\hat{h} + \sigma g\frac{d\hat{h}}{dr}\right)}{\sigma^2 - f^2}, \tag{2.14a}$$

$$\hat{v} = \frac{\left(\frac{n\sigma}{r}g\hat{h} - fg\frac{d\hat{h}}{dr}\right)}{\sigma^2 - f^2}. \tag{2.14b}$$

On making use of (2.11), the PV amplitude is then

$$\begin{aligned}\hat{P} &= \frac{\hat{\zeta}}{H} - f\frac{\hat{h}}{H^2} \\ &= \frac{-gf}{H(\sigma^2 - f^2)}\{\hat{\nabla}^2\hat{h} + \kappa^2\hat{h}\} \\ &= 0.\end{aligned} \tag{2.15}$$

Gravity–inertia waves are thus invisible on PV maps and vorticity is correlated with height

$$\zeta' \propto h'. \tag{2.16}$$

For gravity waves, a rising (falling) free-surface follows convergent (divergent) flow and so mass adjusts to wind

$$\text{mass} \rightarrow \text{wind}. \tag{2.17}$$

Gravity–inertia waves always possess frequencies greater than f, thus

$$\sigma^2 > f^2, \tag{2.18}$$

implying

$$\frac{L^2}{c^2} < \frac{1}{f^2}, \tag{2.19}$$

where again $L = r/n$; yet $c = \sigma r/n$ the azimuthal gravity–inertia wave phase speed. In contrast to Rossby waves, (2.19) indicates if the wave timescale is sufficiently short, the Coriolis force has too little time to rotate the wind vectors and hence mass adjusts to wind. Such wave disturbances are regarded as unbalanced and are customarily identified with the fast manifold.

The geostrophic and gravity–inertia wave solutions constitute a complete basis for the linear problem (2.1) from which an arbitrary initial condition in the height and/or velocity field may be represented and evolved forward in time.

3. Free waves on barotropic vortices: Model formulation

a. Disturbance equations

Having reviewed the free waves on a resting fluid layer, we now investigate the free waves on a circular vortex in gradient balance

$$f\bar{v} + \frac{\bar{v}^2}{r} = g\frac{d\bar{h}}{dr}, \tag{3.1}$$

where $\bar{v} = \bar{v}(r)$ denotes the basic-state tangential wind and $\bar{h} = \bar{h}(r)$ the basic-state free surface height. For small-amplitude disturbances on a stationary vortex, the linearized f-plane momentum and continuity equations are, respectively,

$$\left(\frac{\partial}{\partial t} + \frac{\bar{v}}{r}\frac{\partial}{\partial \lambda}\right)u' - \left(f + \frac{2\bar{v}}{r}\right)v' + g\frac{\partial h'}{\partial r} = 0, \tag{3.2a}$$

$$\left(\frac{\partial}{\partial t} + \frac{\bar{v}}{r}\frac{\partial}{\partial \lambda}\right)v' + \left(f + \frac{d}{rdr}(r\bar{v})\right)u' + g\frac{\partial h'}{r\partial \lambda} = 0, \tag{3.2b}$$

$$\left(\frac{\partial}{\partial t} + \frac{\bar{v}}{r}\frac{\partial}{\partial \lambda}\right)h' + \bar{h}\left(\frac{\partial}{r\partial r}(ru') + \frac{\partial v'}{r\partial \lambda}\right) + u'\frac{d\bar{h}}{dr} = 0. \tag{3.2c}$$

The modal ansatz

$$(u', v', h') = [\hat{u}(r), \hat{v}(r), \hat{h}(r)]\exp[i(n\lambda - \sigma t)] \tag{3.3}$$

again yields a matrix equation

$$\begin{pmatrix} \hat{\sigma} & \tilde{f} & -g\dfrac{d}{dr} \\ \bar{\eta} & \hat{\sigma} & -g\dfrac{n}{r} \\ \dfrac{d}{rdr}[r\bar{h}(\ )] & -\dfrac{n\bar{h}}{r} & \hat{\sigma} \end{pmatrix}\begin{pmatrix} i\hat{u} \\ \hat{v} \\ \hat{h} \end{pmatrix} = \begin{pmatrix} 0 \\ 0 \\ 0 \end{pmatrix}, \tag{3.4}$$

though now $\hat{\sigma} = \sigma - n\bar{\Omega}/r$ denotes the Doppler-shifted frequency, $\bar{\Omega}(r) = \bar{v}/r$ the mean angular velocity, $\bar{\eta} = f + d(r\bar{v})/dr$ the absolute vertical vorticity, and $\tilde{f} = f + 2\bar{\Omega}/r$ the modified Coriolis parameter.

At $r = 0$, perturbation quantities are assumed to be finite, and symmetry considerations require that $d\hat{h}/dr = 0$ for $n = 0$ (symmetric modes) and that $\hat{h} = 0$ for $n \neq 0$ (asymmetric modes). To retain the analog of the two-fold continuum of gravity–inertia waves derived in section 2, we require a vanishing perturbation height field as $r \to \infty$.

b. Discrete eigenvalue problem

Eigenmodes on smooth vortices generally cannot be found by analytical means, so a numerical procedure is adopted. This work discretizes (3.4) and the boundary conditions using second-order centered-difference approximations. The numerical solution technique implements Flatau and Stevens' (1989) numerical primitive equation model, in which discretization is implemented on a staggered grid: $\hat{h}_{2k+1}$ is defined at even grid points $r_{2k} = 2k\delta r$, for $k = 0, 1, 2, \ldots, N$; while $(\hat{u}_{2k}, \hat{v}_{2k})$ is defined at odd grid points $r_{2k-1} = (2k - 1)\delta r$, for $k = 1, 2, \ldots, N$. At odd-numbered grid points, the discrete radial and tangential momentum equations are, respectively:

$$-i\hat{\sigma}_k\hat{u}_k - \tilde{f}_k\hat{v}_k = -g\frac{\hat{h}_{k+1} - \hat{h}_{k-1}}{2\delta r}, \tag{3.5a}$$

$$-i\hat{\sigma}_k\hat{v}_k + \bar{\eta}_k\hat{u}_k = \frac{-ign}{r_k}\frac{1}{2}\left(\hat{h}_{k+1} + \hat{h}_{k-1}\right). \tag{3.5b}$$

At even-numbered grid points, the discrete continuity equation is

$$-i\hat{\sigma}_k\hat{h}_k + \frac{(r\bar{h}\hat{u})_{k+1} - (r\bar{h}\hat{u})_{k-1}}{2r_k\delta r} + \frac{in}{r_k}\bar{h}_k\frac{1}{2}(\hat{v}_{k+1} + \hat{v}_{k-1}) = 0. \tag{3.5c}$$

The radial domain is truncated at an outer radius of 2000 km where $\hat{h}$ is assumed to vanish. The principal features of the eigensolutions discussed below have been verified to be insensitive to the particular choice of outer radius, provided it is at least one external Rossby radius ($\sqrt{gH}/f$). For $n \neq 0$, the boundary condition at $r = 0$ is simply $\hat{h}_1 = 0$. For $n = 0$, the boundary condition at $r = 0$ is $\hat{h}_1 = 4\hat{h}_3/3 - \hat{h}_5/3$, ensuring that $d\hat{h}/dr = 0$ to within second-order accuracy.

The discrete system (3.5) yields a standard matrix-eigenvalue problem,

$$\mathbf{AX} = \sigma\mathbf{X}, \tag{3.6}$$

where σ is the eigenfrequency and the matrix $\mathbf{A}$ represents the discretization of the differential operator (3.5) incorporating the boundary conditions. If N denotes the number of grid intervals for $\hat{h}$, then $\mathbf{X}$ is a column vector consisting of $\{\hat{v}_{2k}, i\hat{u}_{2k}, \hat{h}_{2k+1}\}$ for $k = 1$,

2, 3, . . . , $N - 1$, and $\{\hat{v}_{2N}, i\hat{u}_{2N}\}$ for the next-to-last grid point. The eigenproblem (3.6) is solved with a standard EISPACK routine. Unless otherwise stated, all eigencalculations employ an outer radius of 2000 km and a radial grid increment of $\delta r = 5$ km ($N = 400$). The size of the A matrix is thus 1199×1199. Results shown below have been verified to be converged at this resolution.

c. The basic state: A PV inversion problem

Among the many vortex profiles that could be selected, this work focuses on basic states representative of hurricanes. A distinguishing property of such vortices is the manner in which the azimuthally averaged tangential winds decay with radius in the near-vortex region. To maintain a quasi-steady state under the influence of quadratic surface drag, the near-surface tangential winds in the near-vortex region must decay approximately as the inverse square root of the radius (Riehl 1963; Pearce 1993). Although one may readily construct wind profiles that are consistent with this property and are furthermore inertially (centrifugally) stable, the vortex may still be susceptible to shear instability if the radial PV gradient changes sign. As our objective is to first elucidate the structure of neutral waves in hurricane-like vortices, we limit the $(\bar{v}, \bar{h})$ profiles to be descendants of PV profiles

$$\bar{P} = \frac{1}{\bar{h}}\left[f + \frac{d(r\bar{v})}{rdr}\right], \tag{3.7}$$

which decrease monotonically from the storm center, are positive in the Northern Hemisphere (inertial stability), and exhibit the proper $\bar{v}$ decay in the near-vortex region. For vanishing disturbances at infinity monotonic PV profiles guarantee shear stability in the asymmetric balance (AB) slow manifold (Montgomery and Shapiro 1995).

In defining the basic state, it proves convenient to introduce nondimensional variables indicated by an asterisk:

$$\bar{h} = Hh^*, \qquad r = R_m r^*, \qquad \bar{v} = V_m v^*.$$

Here, H denotes the resting depth, V_m the maximum tangential wind speed, and R_m the radius of maximum tangential winds. Differentiating (3.7) with respect to radius and substituting (3.1) furnishes the nondimensional invertibility problem for $\bar{v}(r)$,

$$\frac{d^2\bar{v}}{dr^2} + \left(\frac{1}{r} - \beta\right)\frac{d\bar{v}}{dr} - \left(\frac{1}{r^2} + \frac{\beta}{r} + \frac{F\bar{P}}{R^2}\right)\bar{v} - \frac{\bar{P}\bar{v}^2}{r}\frac{F}{R} = \frac{\beta}{R}, \tag{3.8}$$

where $\beta = 1/\bar{P}\cdot d\bar{P}/dr$ a normalized basic-state PV gradient, $R = V_m/fR_m$ a Rossby number, and $F = V_m^2/gH$ a squared Froude number. In (3.8) asterisks have been dropped. Solutions are sought subject to the boundary conditions that $\bar{v}(0) = 0$ and that at sufficiently large radius the tangential wind decays as an equivalent point vortex with a deformation radius of $\sqrt{gH}/f$. Mathematically this latter condition takes the form $\bar{v}(r) K_1(\sqrt{F}r/R)$ for $\sqrt{F}r/R \gg 1$, where K_1 is the modified Bessel function of the second kind of order one.

When $R \gg 1$, the nonlinearity of (3.8) prevents analytical solution. Denoting $\bar{v}_i = \bar{v}(r_i)$ where $r_i = i\cdot\delta r$, the solution to the invertibility problem is obtained by relaxation on the quadratic difference equation

$$-\frac{\bar{P}_i\bar{v}_i^2}{r_i}\frac{F}{R} + \frac{\bar{v}_{i+1} - 2\bar{v}_i + \bar{v}_{i-1}}{\delta r^2} + \left(\frac{1}{r_i} - \beta_i\right)\frac{\bar{v}_{i+1} - \bar{v}_{i-1}}{2\delta r} - \left(\frac{1}{r_i^2} + \frac{\beta_i}{r_i} + \frac{\bar{P}_i F}{R^2}\right)\bar{v}_i = \frac{\beta_i}{R}, \tag{3.9a}$$

for $i = 1, 2, \ldots, M - 1$. Of the two possible roots, only one is compatible with geostrophy at large radius. This solution is then subjected to the boundary conditions

$$\bar{v}_0 = 0, \tag{3.9b}$$

$$\frac{\bar{v}_M - \bar{v}_{M-2}}{2\delta r} = \frac{-\sqrt{F}}{R}\bar{v}_{M-1}. \tag{3.9c}$$

The second condition (3.9c) ensures consistency with the asymptotic behavior $\bar{v} \sim K_1(\sqrt{F}r/R)$ for $\sqrt{F}r/R \gg 1$. Since numerical computations must ultimately be confined to a finite domain, experiments have shown that (3.9c) is sufficiently accurate for $r \geq 60$, corresponding to a dimensional outer radius of 3000 km. To be compatible with the resolution of the discrete eigenvalue problem of section 3b an equivalent radial grid increment of $\delta r = 2.5$ km ($M = 1200$) is used in (3.9).

Basic states are then derived from the family of nondimensional PV profiles

$$\bar{P} = 1 + \frac{\alpha_1}{1 + \alpha_2 r^2 + \alpha_3 r^3}, \tag{3.10}$$

where α_1, α_2, and α_3 are adjustable constants. Figure 1a shows four monopolar PV profiles determined suitable for this study. Beginning with the most intense vortex, the constants $(\alpha_1, \alpha_2, \alpha_3)$ used to construct these four profiles are (200, 1, 4), (60, 0.2, 1.0), (8, 0, 0.1), and (2, 0, 0.05), respectively. Solutions to (3.9) were determined convergent when the pointwise residual for (3.8) had maxima less than $O(10^{-8})$. Since the intensity of the vortex could be varied by adjusting the amplitude and radial scale of the PV profile, the nominal Rossby and squared Froude numbers were held fixed at $R = 20$ and $F = 0.25$. These R and F values correspond to a resting fluid depth of $H = 1$ km, a characteristic radius of maximum winds of $r_m = 50$ km, a characteristic tangential velocity of $V_m = 50$ m s^{-1}, and a Coriolis parameter of $f = 5 \times 10^{-5}$ s^{-1}. The resulting dimensional tangential wind and free-surface height for each of the four vortices are shown in Figs. 1b and 1c.

The vortices fall into four intensity regimes. The in-

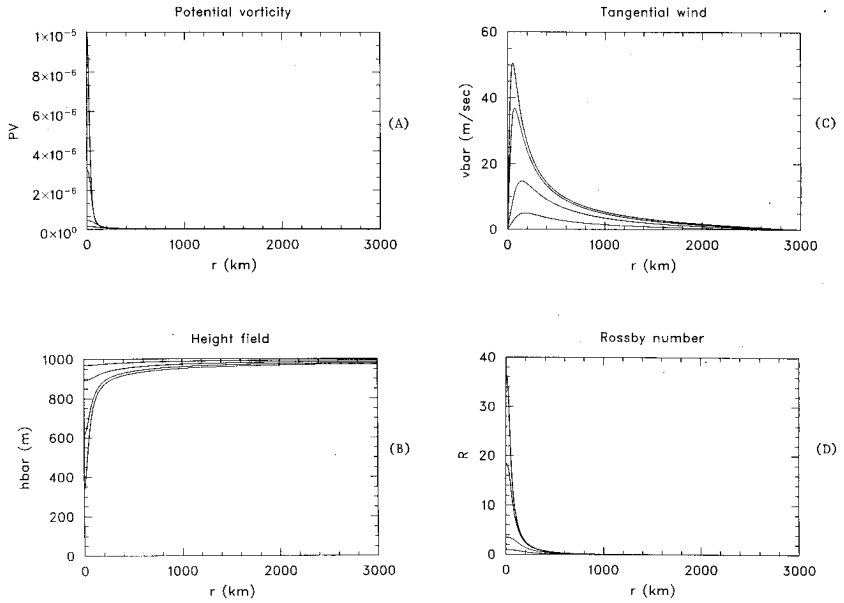

FIG. 1. Basic-state vortex profiles obtained by solving the nonlinear invertibility problem (3.8) for the family of PV monopoles given by (3.10). See text for parameters used. (a) Dimensional PV as a function of radius. Units are $s^{-1}\,m^{-1}$. (b) Dimensional free-surface height h as a function of radius. (c) Dimensional tangential wind $\bar{v}$ as a function of radius. (d) Rossby number $R = \bar{v}/fr$ as a function of radius.

tense hurricane possesses maximum tangential winds of 56 m s^{-1}. The minimal hurricane possesses 37 m s^{-1} maximum tangential winds. The tropical storm possesses 15 m s^{-1} tangential winds, while the incipient vortex has only 5 m s^{-1} tangential winds. Figure 2d plots the Rossby number as a function of radius for each vortex. For much of this paper we concentrate on the minimal hurricane case. A comparison of its tangential wind profile with standard r^{-1} (dotted) and $r^{-1/2}$ (dashed) profiles is shown in Fig. 2. The profile agrees reasonably well with the $r^{-1/2}$ profile for the first 200 km beyond the radius of maximum winds.

Recently, the pioneering study of Broadbent and Moore (1979) examining the interaction of acoustic waves and Rossby edge waves on a Rankine vortex has been extended by Ford (1994) who considered the analogous problem in rotating shallow water. Ford demonstrated that circular Rankine-like vortices possessing a radial discontinuity in basic state PV at the radius of maximum winds are susceptible to mixed Rossby–gravity wave instabilities. In particular, for rapidly rotating cyclonic vortices, Ford showed that high azimuthal wavenumber disturbances become susceptible to mixed instabilities. This is quite unlike quasigeostrophic, or semigeostrophic, balance formulations that guarantee exponential stability for all azimuthal wavenumbers for monotonic PV profiles. Though the corresponding growth rates found by Ford are extremely small throughout the entire (R, F) parameter space (seldom exceeding 10^{-4} inverse turnover times for an inertially stable cyclonic vortex), Ford's work reiterates the inherent fuzziness of the slow manifold concept and raises the possibility that even smooth PV profiles may be susceptible to mixed instabilities. Their somewhat unexpected dependence on azimuthal wavenumber alerts us to the possibility of qualitatively different flow behavior at low and high azimuthal wavenumbers. The present formulation allows further examination of these issues using smooth hurricane-like profiles.

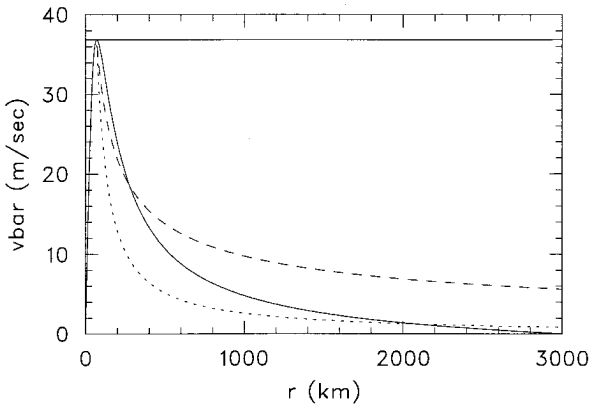

FIG. 2. A comparison of tangential wind profiles for the minimal hurricane vortex and standard r^{-1} (dotted) and $r^{-1/2}$ (dashed) profiles.

4. Vortex eigenfrequencies

For azimuthal wavenumbers 0–10 no unstable eigenfrequencies are found that remain independent of the grid spacing as the grid increment $\delta r \to 0$. Since can-

didate instabilities are found to have associated *e*-folding times of several hundred vortex-turnover times, and because such instabilities disappear upon decreasing δr, we feel confident in concluding that this family of vortices is exponentially stable[1]. Our conclusion is consistent with that of Chan et al. (1993), who, in a related study of two-dimensional compressible vortices, found no instabilities on an *everywhere smooth* basic state consisting of a Gaussian radial vorticity profile.

a. Gravity–inertia waves

Because gravity–inertia wave eigenmodes are found to be smooth eigenfunctions throughout the flow even when the Doppler-shifted frequency vanishes, the corresponding eigenfrequencies are easily distinguished from the Rossby–shear wave eigenfrequencies whose eigenmodes possess a discontinuous tangential velocity at radii where the Doppler-shifted frequency vanishes (see section 5 for further discussion). Figure 3 displays gravity–inertia frequency spectra for azimuthal wavenumbers 0 and 1[1]. Frequencies marked by ○ correspond to a resting basic state, while frequencies marked by × correspond to the minimal hurricane vortex. Both calculations assume a resting depth of 1 km and impose a vanishing height perturbation at $r_{\max} = 2000$ km. Only the first nine eigenfrequencies are shown for both $\sigma < 0$ and $\sigma > 0$.

It is evident from Fig. 3 that axisymmetric ($n = 0$) waves on a vortex possess smaller frequencies than their resting counterparts. The frequency shift is the same for positive and negative eigenfrequencies and the shift is seen to increase with mode number. Nonaxisymmetric waves, on the other hand, display a different behavior. For wavenumber one, retrogressive waves are shifted to lower frequencies than progressive waves. For higher wavenumbers ($n > 2$), retrogressive waves are shifted towards lower frequencies, while progressive waves are shifted towards higher frequencies (not shown).

These frequency characteristics may be qualitatively understood from the local dispersion relation

$$\hat{\sigma}^2 = \bar{f}\bar{\eta} + g\bar{h}(k^2 + n^2/r^2), \tag{4.1}$$

where k is a local *radial* wavenumber, and other notation is defined in section 3. The derivation of (4.1) is based on a WKB approximation which assumes the perturbation radial scale k^{-1} is small compared to the local radial scale of the mean vortex (Hunter 1983, section 4). Although strictly valid for rapidly varying oscillatory modes, (4.1) predicts qualitatively correct results for slowly varying oscillatory modes. In particular, (4.1) implies that

$$\sigma = n\bar{\Omega} \pm \sqrt{\bar{f}\bar{\eta} + gh(k^2 + n^2/r^2)}. \tag{4.2}$$

Thus for axisymmetric modes on a cyclonic vortex, the reduced depth in the near-vortex region causes a reduction in the phase speed and an equal frequency shift for positive and negative frequencies. For nonaxisymmetric waves, retrogressive-wave frequencies are Doppler-shifted to smaller magnitudes, while progressive-wave frequencies are Doppler-shifted to larger magnitudes.

b. Rossby–shear waves

The disturbance equations (3.4) admit an additional class of time-dependent disturbances associated with the shear of the tangential wind. For the simpler problem of rectilinear shear flow in a nondivergent fluid, these waves comprise the well-known sheared disturbances (Thomson 1887; Farrell 1984). In gridpoint models, sheared disturbances are represented by a superposition over a dense but discrete set of eigenfunctions whose frequencies fill the advective interval $[0, n\bar{\Omega}_{\max}]$ (Farrell 1982). Figure 4, for example, shows wavenumber 1, wavenumber 2, and wavenumber 3 eigenspectra for the minimal hurricane vortex. As previously noted no unstable frequencies are evident in these plots. For clarity only frequencies satisfying $|\sigma| < (n + 1)\bar{\Omega}_{\max}$ have been plotted. On comparing Fig. 4 with Fig. 3 the progressive low-frequency gravity waves are embedded in a dense spectrum filling the frequency interval $[0, n\bar{\Omega}_{\max}]$ occupying the real part of the circle whose center lies at $n\bar{\Omega}_{\max}/2$ and whose radius equals $n\bar{\Omega}_{\max}/2$. Because of the nonzero basic-state PV gradient in the near-vortex region, this dense wave spectrum will be referred to as Rossby–shear waves.

5. Vortex eigenmodes

Figure 5a shows a progressively rotating gravity–inertia wave for azimuthal wavenumber 1 whose frequency ($\sigma = 0.968 \times 10^{-3}$ s^{-1}) lies just outside the advective frequency interval. The eigenmode has been normalized to give unit maximum in perturbation geopotential. The dashed curves represent the vortex eigenmode while the solid curves represent the eigenmode's resting counterpart. Not surprisingly, the eigenmode possesses a wavelike structure throughout the vortex including the vortex environment. Despite its distortion relative to its resting counterpart in the near-vortex region, the map plot of Fig. 5b nonetheless exhibits familiar gravity-wave characteristics. Perturbation vorticity is correlated with height, and convergent (divergent) flow is followed by a rising (falling) free surface. The arguments of section 2 imply that

$$\text{mass} \rightarrow \text{wind}.$$

Derived quantities such as PV, divergence, and vorticity are shown in Fig. 5c. In the near-core region, divergence has approximately the same magnitude as vorticity, and at larger radii divergence is even larger than vorticity.

[1] See notes 1 and 2 added in proof, page 1884

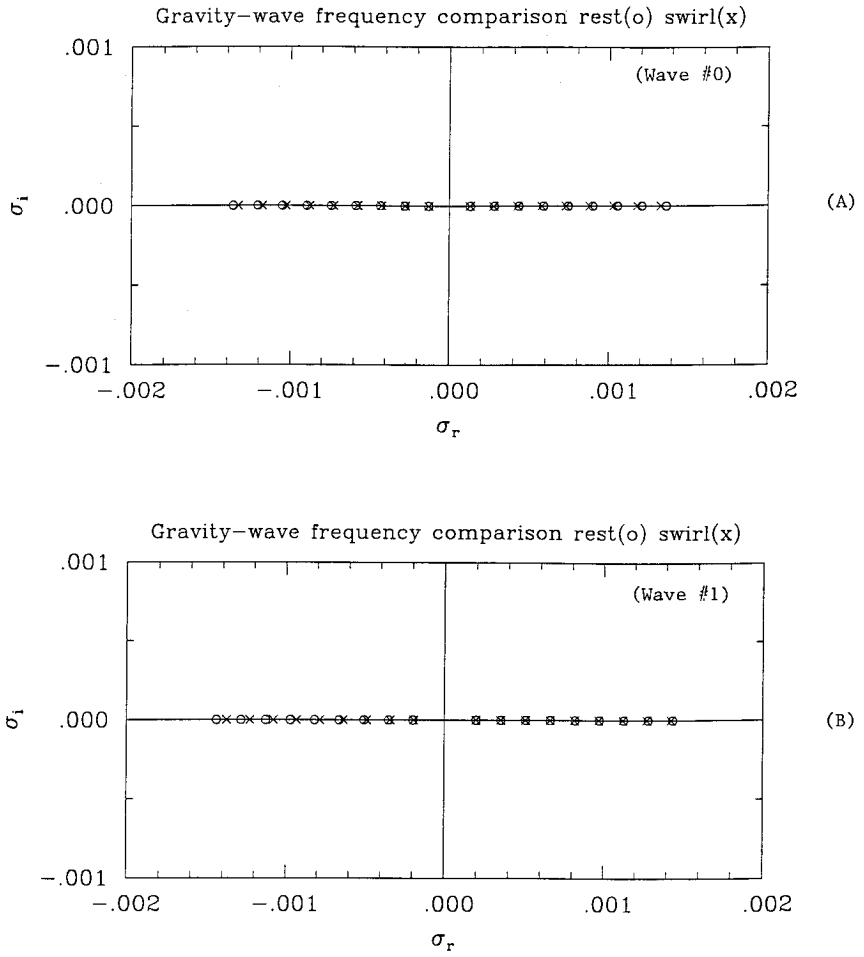

FIG. 3. Frequency comparison of gravity–inertia waves with and without cyclonic swirl. (a) Azimuthal wavenumber zero. (b) Azimuthal wavenumber one. Plotting axes are $Re(\sigma)$ on the abscissa and $Im(\sigma)$ on the ordinate. Frequencies are dimensional and only the first nine modes are shown. Swirling modes are indicated by ×, while resting modes are indicated by ○.

Thus by all conventional measures we would designate this mode a gravity–inertia wave. Higher frequency modes for the same azimuthal wavenumber behave similarly but possess smaller radial wavelengths than shown in Fig. 5a. Unlike gravity–inertia waves on a resting fluid, which have zero disturbance PV, vortex gravity waves possess nonzero PV in the near-core region where $d\bar{P}/dr \neq 0$. Though the amplitude and radial extent of disturbance PV is found to diminish with wave frequency, the fact that such modes are visible on PV maps suggests using solely PV to partition the asymmetric flow into slow and fast components is not a unique procedure.

Figures 6 and 7 illustrate the typical structure of Rossby–shear wave eigenmodes whose frequencies lie within the advective frequency interval $[0, n\bar{\Omega}_{max}]$. The same format of Fig. 5 is adopted. A wavenumber-1 mode is shown in Fig. 6, while a wavenumber-2 mode is shown in Fig. 7. Unlike gravity waves, the radial structure of individual Rossby–shear modes is *not* wavelike. Each mode has a critical level where the Doppler-shifted frequency vanishes. At such points, the perturbation tangential velocity is discontinuous, but the perturbation radial velocity and geopotential are continuous as required by kinematic and dynamic boundary conditions at the critical level. Each mode is a discrete approximation to one of the continuum of singular neutral modes in the continuous formulation whose superposition describes sheared disturbances (Farrell 1982). For the problem of rectilinear simple-shear flow there is no basic state vorticity gradient. The corresponding shear eigenmodes consequently possess a delta function in vorticity at the critical level, yet are irrotational elsewhere. In circular vortices possessing a smooth radial gradient in basic-state PV, however, shear modes possess nonzero disturbance PV in regions where $d\bar{P}/dr \neq 0$ (see Figs. 6c and 7c).

Looking closely at Figs. 6b and c, several features stand out. First, as the wave propagates around the vortex center wind follows height, that is,

$$\text{wind} \rightarrow \text{mass}.$$

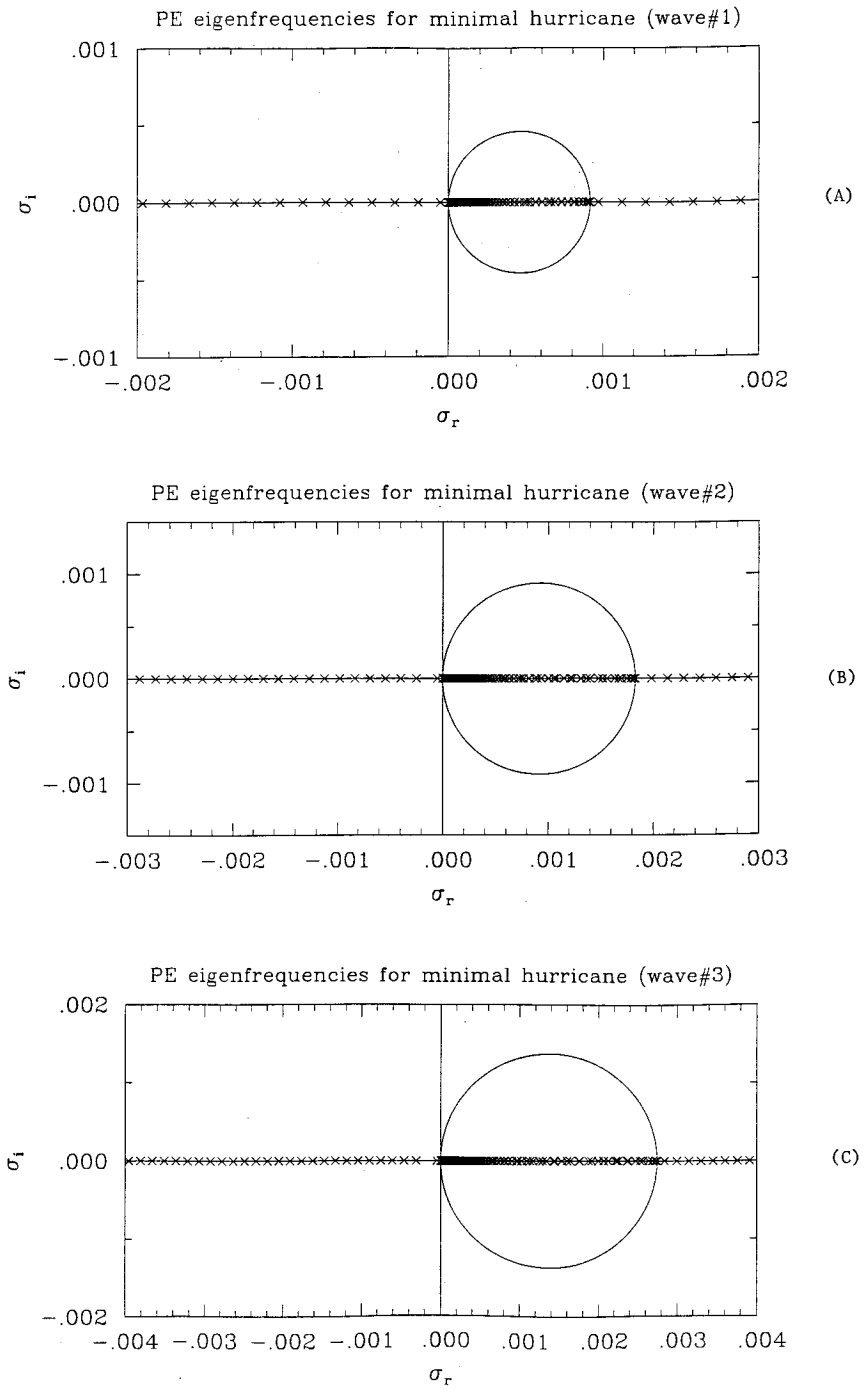

FIG. 4. Frequency scatterplots for the minimal hurricane vortex. Gravity–inertia wave and Rossby–shear wave eigenfrequencies are both indicated by X. Only frequencies satisfying $|\sigma| < (n + 1)\Omega_{max}$ are shown, where n is azimuthal wavenumber. (a) Azimuthal wavenumber 1. (b) Azimuthal wavenumber 2. (c) Azimuthal wavenumber 3.

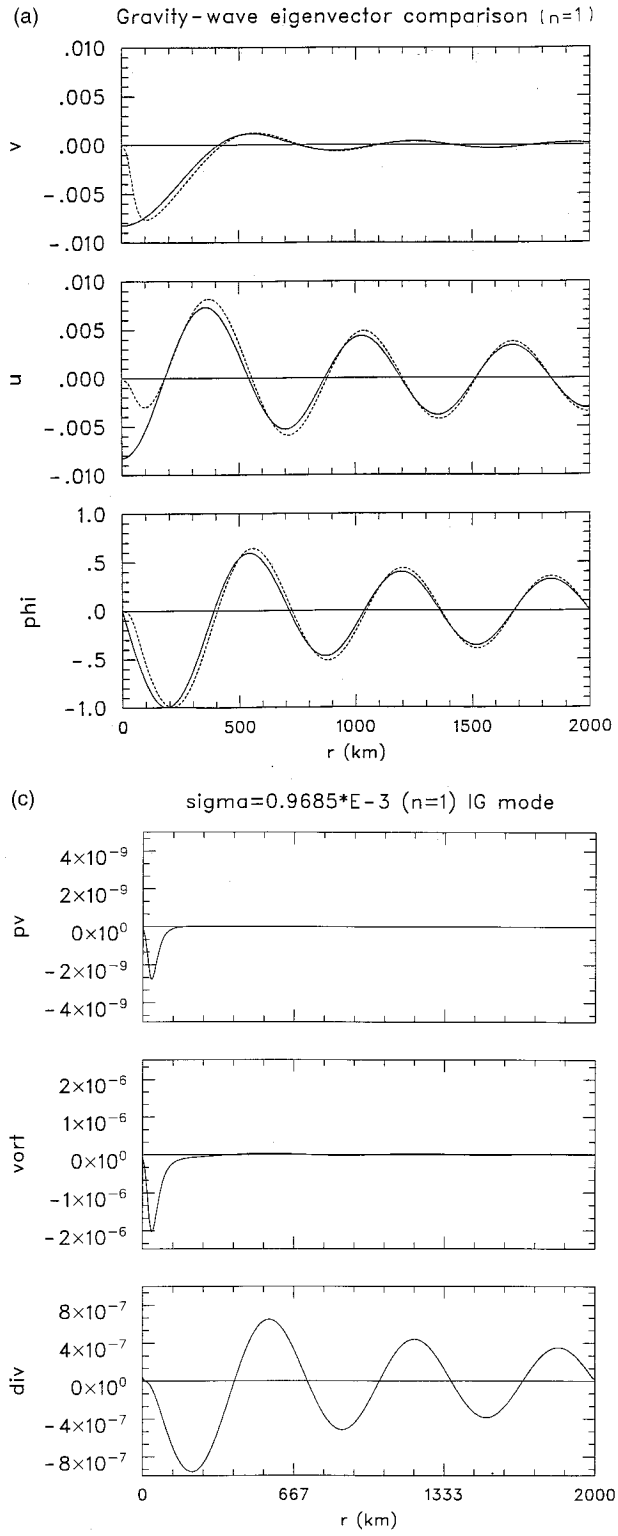

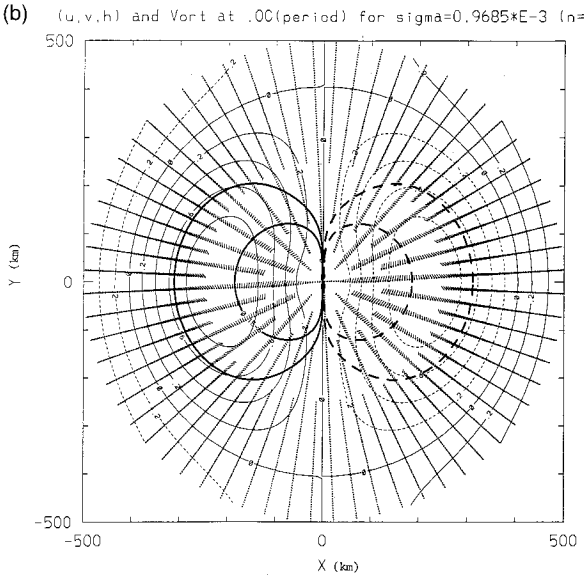

FIG. 5. Progressive gravity–inertia wave ($\sigma = 0.968 \times 10^{-3}$ s^{-1}) for azimuthal wavenumber 1. (a) Radial structure for $\hat{v}(r)$, $i\hat{u}(r)$, and $\hat{\Phi}(r)$. The vortex mode is indicated by the dashed plot, while its resting counterpart is indicated by the solid plot. (b) Map plot. Perturbation winds are indicated with vectors. Light solid and dashed lines denote positive and negative perturbation height contours, respectively. Heavy solid and dashed lines denote perturbation vorticity contours. (c) Radial structure for $\hat{PV}(r)$, $\hat{\zeta}(r)$, and divergence amplitude $\hat{\delta}(r)$ for vortex eigenmode. The eigenvector $\hat{v}(r)$, $i\hat{u}(r)$, $\hat{\Phi}(r)$ has been normalized to give unit maximum in perturbation geopotential.

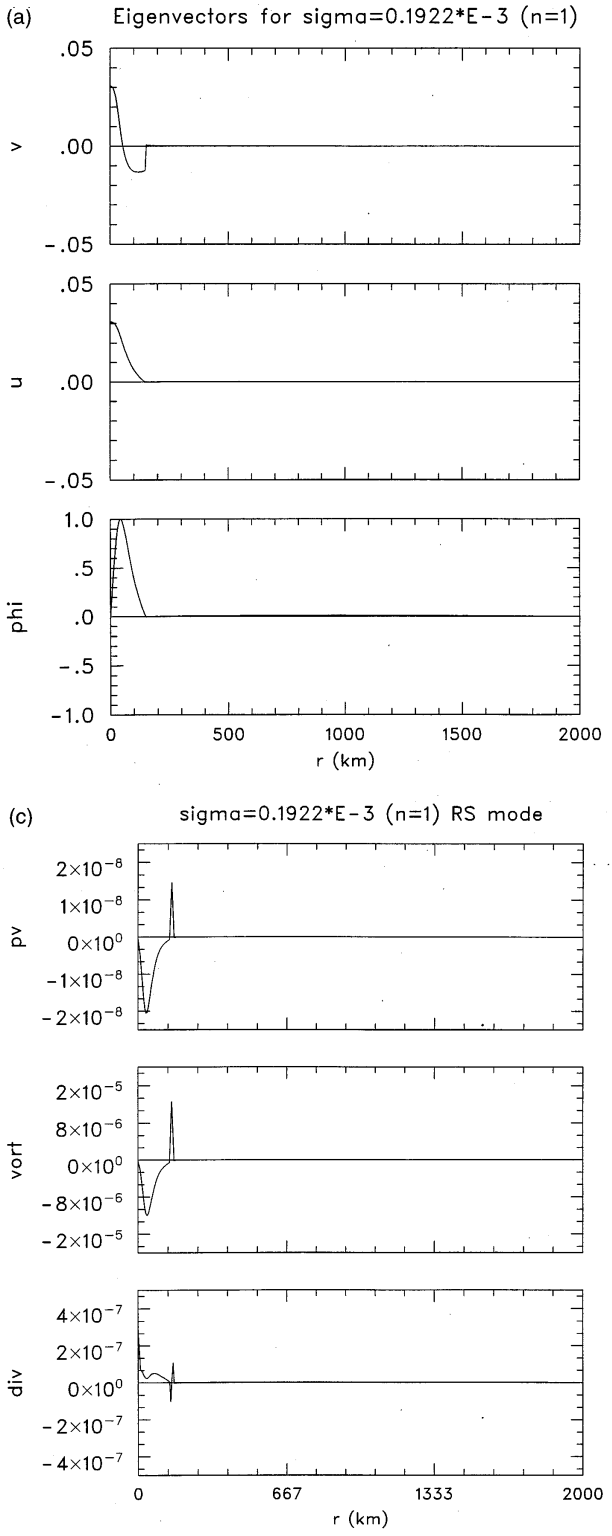

FIG. 6. Rossby–shear mode ($\sigma = 0.1922 \times 10^{-3}$ s^{-1}) for azimuthal wavenumber 1. Plotting convention is as in Fig. 5.

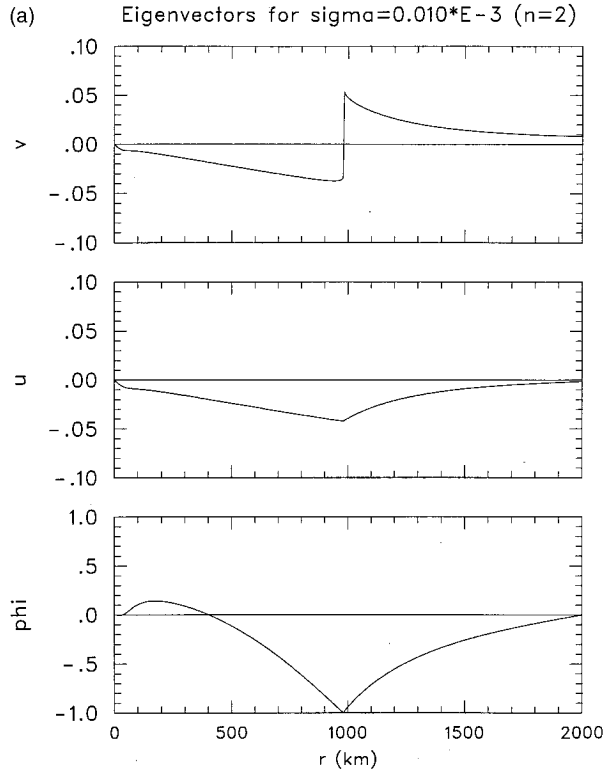

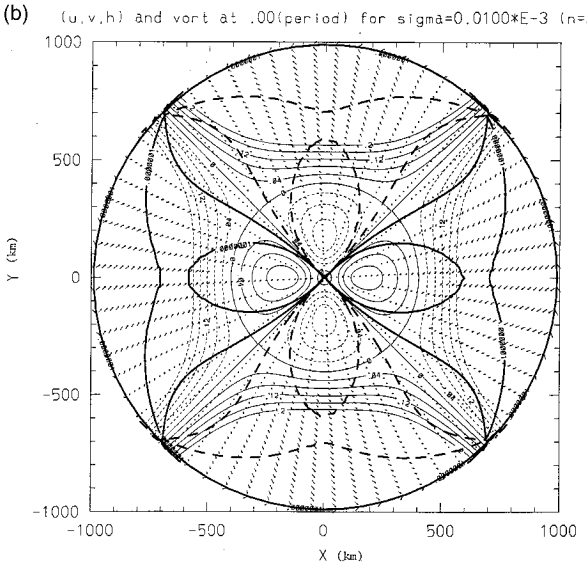

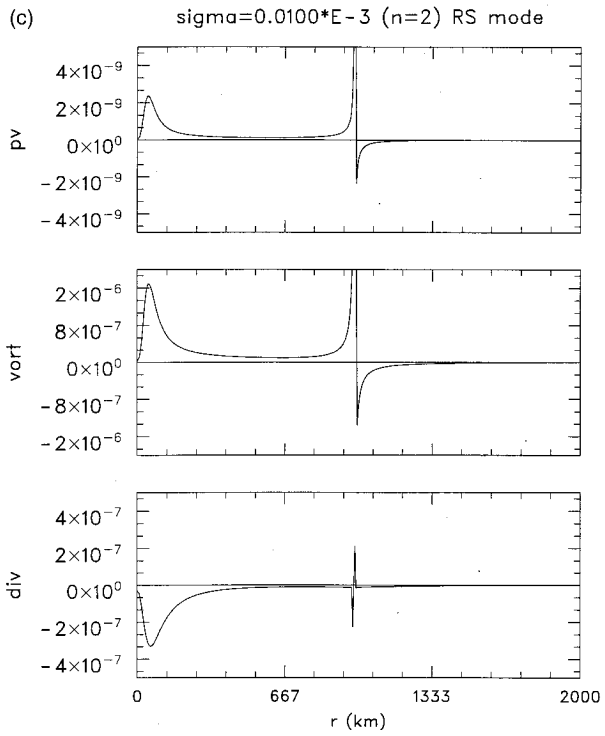

FIG. 7. Rossby–shear mode ($\sigma = 0.01 \times 10^{-3}$ s^{-1}) for azimuthal wavenumber 2. Plotting convention is as in Fig. 5.

Second, within the region bounded by the critical level vorticity and height are anticorrelated,

$$\zeta' \propto -h'.$$

Finally, Fig. 6c indicates that vorticity is approximately fifteen times greater than divergence within this same region. Thus by conventional measures one may regard this mode as balanced. Other wavenumber-1 Rossby-shear modes behave similarly.

At higher wavenumbers ($n \geq 2$), we observe both expected and unexpected features. Figure 7, for example, shows a wavenumber-2 Rossby–shear mode having its critical level near $r = 975$ km. Like the previous shear wave example, the radial structure is not wavelike. At the critical level, the tangential velocity is discontinuous, while the radial velocity and geopotential are continuous. Within the region bounded by the critical level but beyond approximately 400 km from the vortex center the height field and vorticity field are anticorrelated,

$$\zeta' \propto -h';$$

perturbation winds are anticyclonic (cyclonic) where perturbation heights are positive (negative); and vorticity is more than an order of magnitude larger than the divergence. In the vortex environment (away from the core region) this mode can thus be regarded as balanced. This is to be expected since both Rossby and Froude numbers are small compared to unity[2] for $r \gg R_m$.

In the near-core region unexpected structure changes are found. Within 400 km of the vortex center, the height field and vorticity field become correlated,

$$\zeta' \propto h',$$

and divergence is only a factor of 4–5 smaller than vorticity. To verify this is not a coincidence, PV, vorticity, and divergence amplitudes for wavenumber-3 Rossby–shear modes were also examined but are not shown here. For Rossby–shear modes possessing their critical levels far from the near-core region, the divergence becomes only a factor of 2 smaller than vorticity in the near-core region, and radial plots of $\hat{h}$ again show them to be correlated with vorticity there. The tendency for divergence to become comparable to vorticity for higher wavenumber Rossby–shear modes has also been verified for wavenumber-4 Rossby–shear modes. Because the squared Froude number is approximately 0.2 in the near-core region, the disparity between vorticity and divergence for wavenumber 1 is not at all surprising. However, the emergence of gravity-wave-like behavior in the near-core region for the advective modes at higher wavenumbers is not anticipated by simple scaling arguments depending solely on external parameters such as the squared Froude number (McWilliams 1985). The

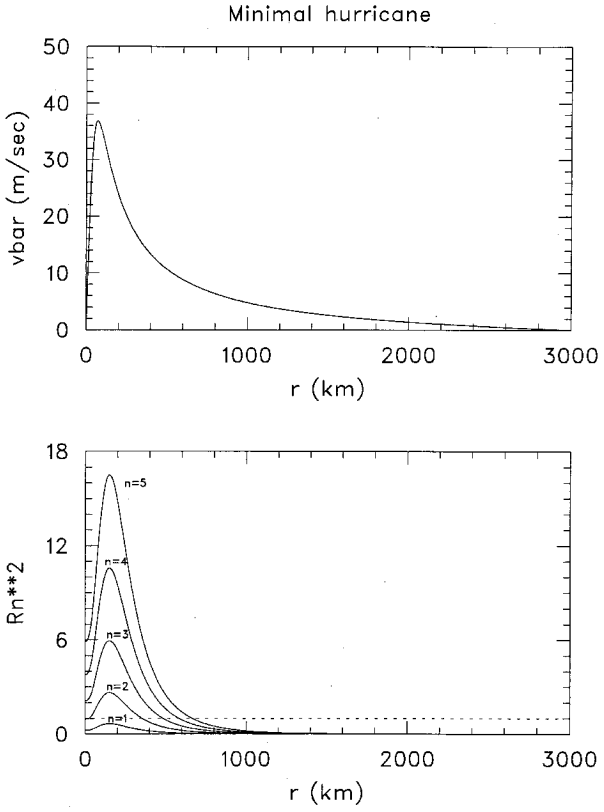

FIG. 8. Local Rossby number squared $R_n^2(r)$ for the minimal hurricane vortex.

mixed wave structure of Fig. 7b is reminiscent of mixed Rossby–gravity waves (Yanai waves) found on the equatorial beta plane (Matsuno 1966).

These unexpected structure changes can be understood physically upon considering the generalization of the Rossby adjustment argument of section 2 to a rapidly rotating vortex in gradient balance. On substituting

$$f^2 \leftarrow \tilde{f}\,\overline{\eta},$$
$$c^2 \leftarrow \overline{v}^2, \tag{5.1}$$

the condition for balanced behavior (2.10) becomes

$$\frac{n^2\overline{v}^2}{\tilde{f}\,\overline{\eta}r^2} < 1. \tag{5.2}$$

The left side of the inequality is simply the square of the local Rossby number for wavenumber n (Shapiro and Montgomery 1993). Figure 8 shows R_n^2 as a function of radius for the minimal hurricane vortex. Figure 8 suggests that only wavenumber-1 Rossby–shear modes can be considered balanced throughout the near-core region and the vortex environment. The local Rossby number for wavenumbers $n \geq 2$ is greater than unity in a substantial portion of the near-vortex region. Consistent with this finding, we observe that, within 400 km where $R_2^2 > 1$, height and vorticity

[2] See note 3 added in proof, page 1884

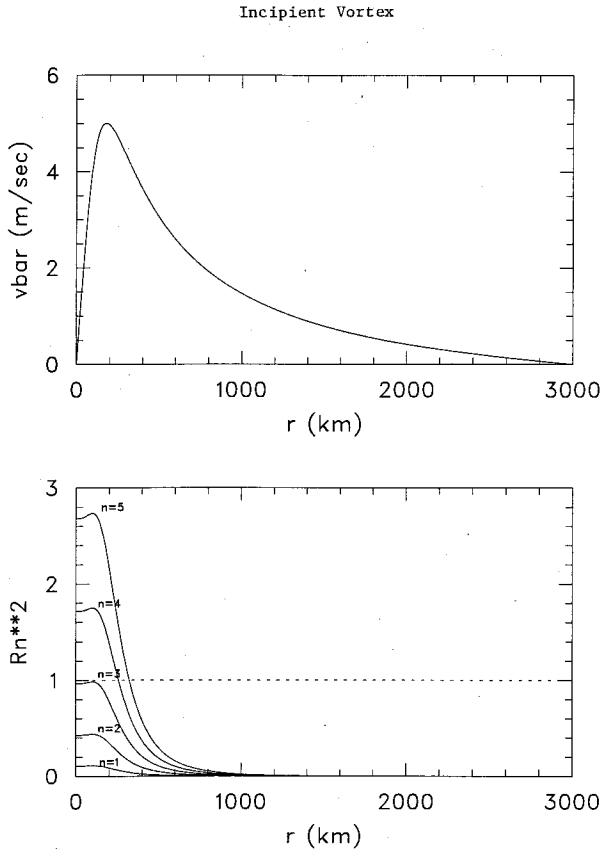

FIG. 9. Local Rossby number squared $R_n^2(r)$ for the incipient vortex.

fields are correlated (cf. Fig. 7b). Similar consistency has been verified for wavenumber three and higher modes.

The robustness of the balance criterion (5.2) has been tested for the other vortex profiles of section 3c. As an example, Fig. 9 plots R_n^2 as a function of radius for the incipient vortex. It is evident that R_n^2 is uniformly less than unity throughout the vortex and its environment for $n \leq 3$. For $n \geq 4$, however, the criterion predicts mixed-mode behavior in the near-core region. Figures 10a and 10b confirm this prediction by showing an example of a Rossby–shear mode for $n = 3$ and $n = 4$, respectively. For $n = 3$, vorticity is anticorrelated with height throughout the near-core region bounded by the critical region, while for $n = 4$, vorticity is correlated with height in the same region. Physically, high wavenumber disturbances possess a smaller length scale than the basic-state circular vortex. Consequently, scaling considerations that presume the existence of a single length scale characterizing the slow manifold, such as McWilliams (1985) or Spall and McWilliams (1992), are no longer appropriate (M. Spall 1996, personal communication).

The more general implementation of (2.10) encompassing both low and high frequencies within the advective range $0 \leq \sigma \leq n\bar{\Omega}_{\max}$ considers the Doppler-shifted phase velocity relative to the local tangential wind $\bar{v}$. In this case one substitutes

$$f^2 \leftarrow \tilde{f}\,\bar{\eta},$$

$$c^2 \leftarrow \left(\frac{\sigma r}{n} - \bar{v}\right)^2, \tag{5.3}$$

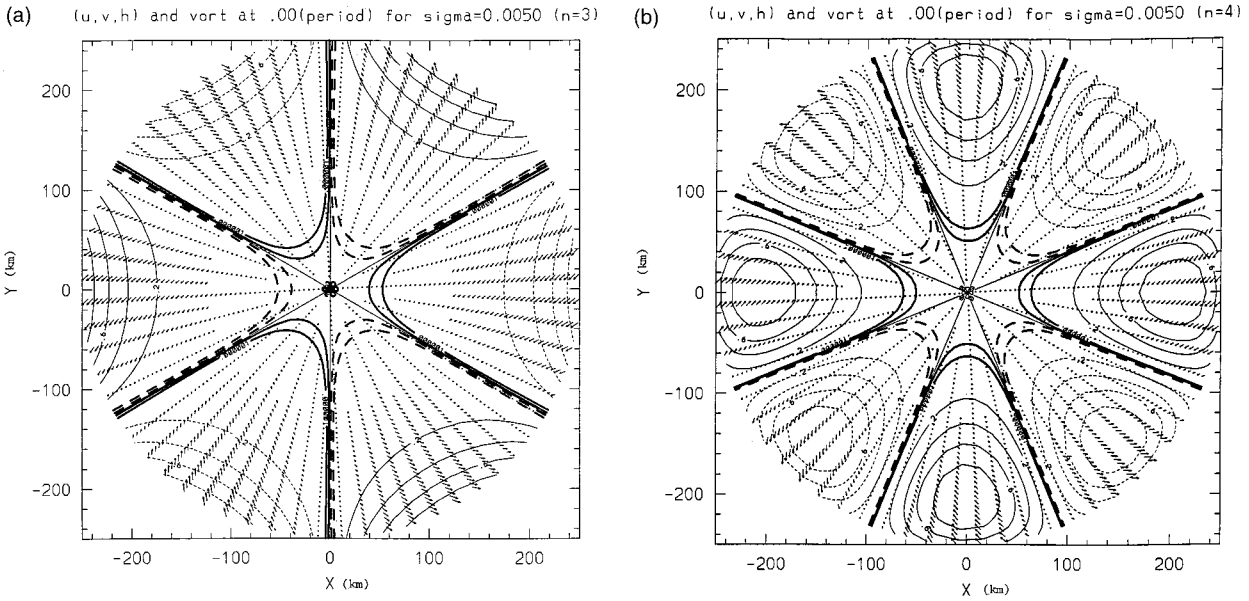

FIG. 10. Rossby–shear map plots for the incipient vortex. (a) Rossby–shear mode ($\sigma = 0.005 \times 10^{-3}$ s^{-1}) for azimuthal wavenumber 3. (b) Rossby–shear mode ($\sigma = 0.005 \times 10^{-3}$ s^{-1}) for azimuthal wavenumber 4. Plotting convention is as in Fig. 5.

to obtain the generalized criterion for balanced behavior in the near-core region:

$$\frac{(\sigma - n\bar{\Omega})^2}{\tilde{f}\,\bar{\eta}} < 1, \tag{5.4}$$

where $\bar{\Omega} = \bar{v}/r$ is the basic state angular velocity. Denoting D^2 as the ratio of the advective accelerations following the circular vortex to the inertial stability (Shapiro and Montgomery 1993), the left-hand side of (5.4) is recognized as D^2 for frequency σ and azimuthal wavenumber n. Eigenmodes whose eigenfrequencies reside in the advective range with magnitudes closer to $n\bar{\Omega}_{\max}$ have also been examined. In this case, the eigenmodes exhibit balanced characteristics in regions where $D^2 < 1$, whereas in regions where $D^2 > 1$, the eigenmodes exhibit gravity-wave characteristics. As a result, modes that behave like gravity waves in the vortex environment display balanced behavior in the near-core region.

6. Radiating gravity–inertia and vortex–Rossby waves

Having characterized the vortex eigenmodes for circular vortices with smooth and monotonic PV profiles, we now briefly consider the initial-value problem. Our goals here are twofold. First, we provide evidence that the eigenmodes so constructed comprise a complete basis for the linear dynamics defined by (3.2). Second, with a simple initial condition we show that the nonaxisymmetric adjustment process typically consists of radiating gravity–inertia waves and vortex–Rossby waves. A more in-depth study of the nonaxisymmetric adjustment problem will be reported in a forthcoming publication.

As is usual in linear dynamics, the general solution for wavenumber n is written as a superposition over all possible eigenmodes for wavenumber n. Recalling the staggered grid arrangement defined in section 3b, at the N velocity grid points (r_j; $= 1, 3, 5, \ldots, 2N - 1$) we write

$$\hat{u}(r_j, t) = \sum_{k=1}^{3N-1} C_k \hat{u}_{j,k} \exp(-i\sigma_k t), \tag{6.1a}$$

$$\hat{v}(r_j, t) = \sum_{k=1}^{3N-1} C_k \hat{v}_{j,k} \exp(-i\sigma_k t), \tag{6.1b}$$

whereas at the $N - 1$ height grid points (r_j; $j = 2, 4, 6, \ldots, 2N - 2$) we write

$$\hat{h}(r_j, t) = \sum_{k=1}^{3N-1} C_k \hat{h}_{j,k} \exp(-i\sigma_k t). \tag{6.1c}$$

Here, ($\hat{u}_{j,k}$, $\hat{v}_{j,k}$, $\hat{h}_{j,k}$) represent components of the eigenvectors for wavenumber n as defined in section 3b, where j is the radial index and k is the eigenfrequency index. For a given initial condition [$\hat{u}(r_j, 0)$, $\hat{v}(r_j, 0)$, $\hat{h}(r_j, 0)$] the coefficients (C_k) are determined by inverting the linear system (6.1). The system is well posed and represents $3N - 1$ equations in $3N - 1$ unknowns. Keeping with the parameters of section 3, we choose $N = 400$, which yields a coefficient matrix with 1199×1199 elements. The solution to (6.1) has been successfully implemented on the National Center for Atmospheric Research (NCAR) Cray-Y-MP using a standard EISPACK routine for a variety of initial conditions. Although the successful inversion of (6.1) does not constitute a rigorous proof that the vortex eigenmodes form a complete set, the numerical evidence suggests this is indeed the case at least for localized initial disturbances.

As an example of the evolutionary dynamics implied by (6.1), we consider a windless initial condition for an azimuthal wavenumber-1 disturbance on the minimal hurricane vortex,

$$\hat{h}(r, 0) = b_1 r \exp\left[\left(-\frac{r}{\gamma R_m}\right)^2\right], \tag{6.2}$$

where $b_1 = \sqrt{2e}/\gamma R_m$, $\gamma = 2$, and $R_m = 50$ km. As evident from the recipe, $\hat{h}$ vanishes at $r = 0$ and is consistent with the boundary condition there. The height perturbation is dimensionalized in order to attain a maximum amplitude of 10 m at $r = \gamma R_m/\sqrt{2}$.

Figure 11 highlights the salient features of the solution. Shown are snapshots of the perturbation height (Figs. 11a,b) and PV (Figs. 11c,d) at $t = 0.0$, 3.25, and 5.0 h. Figures 11a and 11b show an outward propagating gravity–inertia wave packet that quickly separates from the near-core region. Since the basic-state radial PV gradient is effectively zero beyond 400 km, this wave packet becomes invisible on PV maps at distant radii. The radial group velocity with which the wave packet propagates has been verified to equal $\sqrt{gH}$ (99 m s^{-1}). The secondary wave packet just behind the leading packet is associated with inward propagating gravity waves that become outward propagating gravity waves upon reaching the vortex center. Analysis confirms that the leading edge of the wave packet can be accurately depicted as an outward propagating trailing spiral (the dashed line in Fig. 11a). For $t \geq 3$ h, a least squares calculation for the leading edge of the packet gives

$$h'(r, \lambda, t) = \mathrm{Re}\{\exp\langle i[k(r - R) + n\lambda]\rangle\}, \tag{6.3}$$

where $k = 2.16 \times 10^{-2}$ rad km^{-1}, and $R = 1136.4$ km $+ \sqrt{gH}(t - 3$ h). In (6.3) the $1/\sqrt{R}$ geometrical factor that usually multiplies (6.3) in cylindrical geometry has been neglected because of its weak variation over the distance considered. The simulation was terminated at $t = 5$ h because the gravity wave reached the outer boundary at 2000 km soon after this time. The features thus described have been verified with an independent linear PE simulation employing grid points radially and Fourier modes azimuthally. Hence, although each gravity–inertia eigenmode of

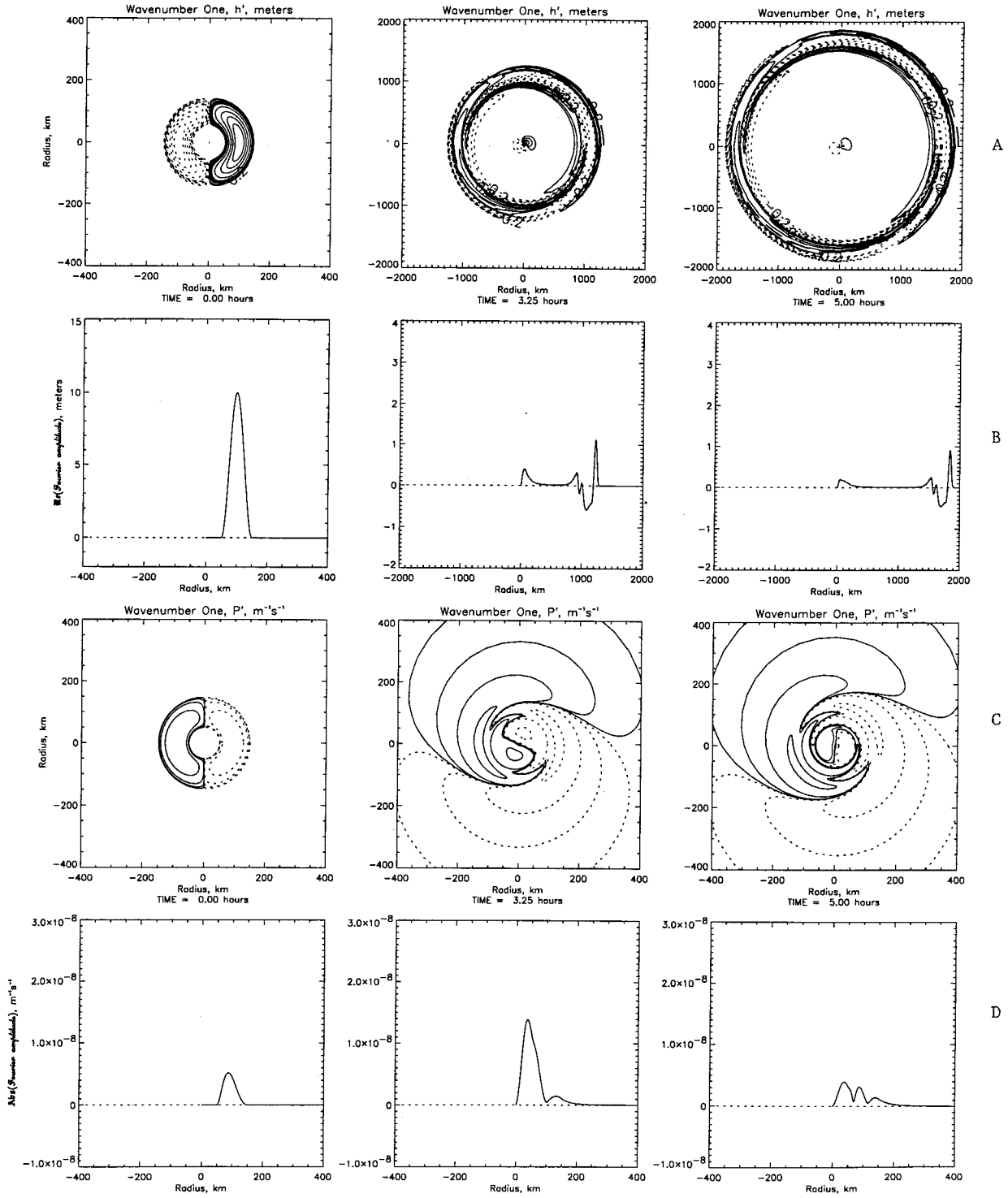

FIG. 11. Snapshots of perturbation height and PV highlighting the nonaxisymmetric adjustment process obtained by summing the vortex eigenmodes for the minimal hurricane vortex. The initial condition is the wavenumber-1 height disturbance (6.2). (a) Map-plots of perturbation height at time $t = 0.0$, 3.25, and 5.0 h. (b) Radial-profile plots of perturbation height along $\lambda = 0$ at the same times of (a). (c) Map-plots of perturbation PV at the same times of (a). Contour intervals are $\pm 10^{-7}$, 10^{-8}, . . . , 10^{-12} s^{-1} m^{-1}. (d) Radial profile of $|\widehat{PV}|$ at the same times of (a). Note the reduced domain size in (c) and (d).

section 5 represents a standing wave in the radial direction, superposing them correctly captures inward and outward wave propagation.

Following the rapid emission of gravity–inertia waves, Figs. 11c,d reveal vortex–Rossby waves (PV waves) in the near-core region that begin to get sheared by the differential rotation of the mean vortex. Previous work (Montgomery and Kallenbach 1997) has already developed the basic theory for these waves in the context of nondivergent and asymmetric-balance vortex dynamics. The relevant features to note in Figs. 11c,d are outward-propagating PV wave packets and the emergence of the steady-state pseudo-mode near $r = 0$ indicating the displacement of the vortex. Unlike gravity–inertia waves, vortex–Rossby waves are tied to the near-vortex region where the radial PV gradient is nonzero. Although each Rossby–shear eigenmode does not propagate radially, superposing them correctly captures inward and outward wave propagation.

7. Conclusions

Previous work has examined the physics of vortex axisymmetrization using idealized nondivergent and asymmetric balance models (Montgomery and Kallenbach 1997, and references therein). To quantify the role of radiating gravity–inertia waves and vortex–Rossby waves in the ensuing wave-mean-flow dynamics of the primitive equations, one must first understand the structure of nonaxisymmetric waves in the primitive equations. As a first step towards tackling the more complex nonaxisymmetric adjustment problem in inviscid and swirling boundary-layer vortex flows, the complete wave spectrum in barotropic shallow water vortices representative of hurricane-like flows has been investigated here. Armed with an understanding of the free waves on a resting fluid in an unbounded domain, eigenfrequencies and eigenfunctions were examined for hurricane-like vortices. Eigensolutions are found to fall into two continuum classes.

Eigenmodes possessing frequencies greater than the maximum advective frequency for azimuthal wavenumber n are modified gravity–inertia waves that propagate around the vortex. Changes in the gravity-wave spectra were accounted for using simple WKB theory. Unlike gravity–inertia waves in a resting fluid layer, vortex gravity–inertia waves are no longer invisible to the PV dynamics in the near-core region.

Classification of modes with frequencies less than or equal to the advective frequency (''advective modes'') is more subtle. In addition to the continuous spectrum of gravity–inertia waves, the continuous spectrum of Rossby–shear waves comprises the second class of disturbances. Rossby–shear waves possess critical levels where the Doppler-shifted frequency vanishes and also possess disturbance PV in regions where the radial PV gradient is nonzero. Although no exponentially unstable modes are found for the class of smooth monopolar PV profiles considered here, we find that both vortex structure and azimuthal wavenumber govern whether the advective modes may be identified as balanced (''slow'') or unbalanced (''fast'') in the near-vortex region. A simple criterion generalizing Rossby's characterization of balanced and unbalanced flow to that of azimuthal wave disturbances on a circular vortex was proposed for monochromatic disturbances that is consistent with AB theory (Shapiro and Montgomery 1993). Consistent with the scaling predictions of AB theory, Rossby–shear waves on monopolar vortices exhibit gravity–wave-like characteristics in the near-core region when the *local* Rossby number for wavenumber n is greater than unity. This structure change is not anticipated by traditional scaling arguments using solely external flow parameters such as the squared Froude number and is reminiscent of the mixed Rossby–gravity waves found on an equatorial beta plane (Matsuno 1966). The implication of such structure changes in the nonaxisymmetric adjustment process is the subject of current work that will be reported in a forthcoming publication.

Note 1 added in proof (see page 1874). We believe our conclusion is valid for the unbounded domain, which is approximated here by vanishing height perturbations at $r = a$. On further inspection of our results a weakness of this formulation was noted through the discovery of a pure inertial oscillation with frequency $\sigma = -f$ and uniform or increasing wind amplitudes near $r = a$. When the eigenvalue problem (3.6) was reformulated with the boundary condition $u' = 0$ at $r = a$, this inertial mode disappeared altogether yet the other results of sections 4 and 5 were essentially unaffected. The drawback of this latter condition, however, is the excitation of spurious boundary inabilities associated with Kelvin edge-waves on $r = a$ which have no counterpart in the infinite domain problem and only complicate the physical interpretations.

Note 2 added in proof (see page 1874). The displayed vortex gravity–inertia eigenfrequencies have been verified to approximate a twofold continuum by increasing the domain size while keeping the number of grid points constant and observing that the eigenfrequencies become more closely spaced.

Note 3 added in proof (see page 1880). At sufficient distances beyond the critical level h' cannot remain anticorrelates with ζ' because the perturbation PV ultimately vanishes. At such distances $\zeta' = fh'|H$ but the mode is nevertheless balanced since the perturbation winds are nearly geostrophic.

Acknowledgments. This research was supported in part by the National Science Foundation Grant ATM-9312655 and the Office of Naval Research Grant N00014-93-1-0456. The monochromatic adjustment criterion was inspired by conversations with Dr. Wayne Schubert. The authors wish to thank Dr. Michael Spall,

Dr. T. Warn, and two anonymous reviewers for their constructive comments on the original manuscript. The PE eigenmode model is based on the model developed by Dr. Duane Stevens, Dr. Maria Flatau, and Mr. Paul Ciesielski at Colorado State University. Figures were constructed using Mr. Jim Edwards's plotting program and we thank Mr. Dave Stepaniak for carrying out the calculation of section 6, which formed part of his M.S. thesis (Stepaniak et al. 1996).

REFERENCES

Broadbent, E. G., and D. W. Moore, 1979: Acoustic destabilization of vortices. *Philos. Trans. Roy. Soc. London, Ser. A,* **290,** 353–371.

Chan, W. M., K. Shariff, and T. H. Pulliam, 1993: Instabilities of two-dimensional inviscid compressible vortices. *J. Fluid Mech.,* **253,** 173–209.

Dewar, W. K., and P. D. Killworth, 1995: On the stability of oceanic rings. *J. Phys. Oceanogr.,* **25,** 1467–1487.

Farrell, B. F., 1982: The initial growth of disturbances in a baroclinic flow. *J. Atmos. Sci.,* **39,** 1663–1686.

——, 1984: Modal and non-modal baroclinic waves. *J. Atmos. Sci.,* **41,** 668–673.

Flatau, M., and D. E. Stevens, 1989: Barotropic and inertial instabilities in the hurricane outflow layer. *Geophys. Astrophys. Fluid Dyn.,* **47,** 1–18.

Ford, R., 1994: The instability of an axisymmetric vortex with monotonic potential vorticity in rotating shallow water. *J. Fluid Mech.,* **280,** 303–334.

Fung, I. Y., 1977: The organization of spiral rainbands in a hurricane. Ph.D. dissertation, Massachusetts Institute of Technology, 140 pp.

Gill, A. E., 1982: *Atmosphere–Ocean Dynamics.* Academic Press, 662 pp.

Hunter, C., 1983: Galactic dynamics. *Lect. Appl. Math.,* **20,** 199–203.

Kurihara, Y., 1976: On the development of spiral bands in a tropical cyclone. *J. Atmos. Sci.,* **33,** 940–958.

Lindzen, R. D., 1967: Planetary waves on beta-planes. *Mon. Wea. Rev.,* **95,** 441–451.

Longuet-Higgins, M. S., 1968: The eigenfunctions of Laplace's tidal equations over a sphere. *Philos. Trans. Roy. Soc. London, Ser. A,* **262,** 511–607.

Matsuno, T., 1966: Quasi-geostrophic motions in the equatorial area. *J. Meteor. Soc. Japan,* **44,** 25–43.

McWilliams, J. C., 1985: A uniformly valid model spanning the regimes of geostrophic and isotropic, stratified turbulence: Balanced turbulence. *J. Atmos. Sci.,* **42,** 1773–1774.

Montgomery, M. T., and L. J. Shapiro, 1995: Generalized Charney–Stern and Fjortoft theorems for rapidly rotating vortices. *J. Atmos. Sci.,* **52,** 1829–1833.

——, and R. J. Kallenbach, 1997: A theory for vortex Rossby waves and its application to spiral bands and intensity changes in hurricanes. *Quart. J. Roy. Meteor. Soc.,* **123,** 435–465.

Pearce, R. P., 1993: A critical review of progress in tropical cyclone physics including experimentation with numerical models. *Tropical Cyclone Disasters. Proceedings of the ICSU/WMO International Symposium,* Peking University Press, 45–60.

Phillips, N. A., 1965: Elementary Rossby waves. *Tellus,* **XVII,** 295–301.

Riehl, H., 1963: Some relations between wind and thermal structure of steady state hurricanes. *J. Atmos. Sci.,* **20,** 276–287.

Shapiro, L. J., and M. T. Montgomery, 1993: A three-dimensional balance theory for rapidly rotating vortices. *J. Atmos. Sci.,* **50,** 3322–3335.

Spall, M. A., and J. C. McWilliams, 1992: Rotational and gravitational influences on the degree of balance in the shallow-water equation. *Geophys. Astrophys. Fluid Dyn.,* **64,** 1–29.

Stepaniak, D., W. Schubert, and M. T. Montgomery, 1996: An initial-value problem study of free waves on a barotropic vortex. Atmospheric Science Bluebook #600, 74 pp.

Thomson, W., 1879: On gravitational oscillations of rotating water. *Proc. Roy. Soc. Edinburgh,* Session 1878–79, 92–99.

——, 1887: Stability of fluid motion: Rectilinear motion of viscous fluid between two parallel planes. *Philos. Mag.,* **24,** 188–196.

Willoughby, H. E., 1977: Inertia-buoyancy waves in hurricanes. *J. Atmos. Sci.,* **34,** 1028–1039.